High-Temperature Microstructural Evolution and Quantification for Alloys IN740 and IN740H: a Comparative Study

S.F. Di Martino*†, R.G. Faulkner*, S.C. Hogg*

† Corresponding author; Tel. +44 01509 263171, Ext.: 4361; e-mail S.F.Di-Martino@outlook.com
* Department of Materials, Loughborough University, LE11 3TU, UK

ABSTRACT

In the context of ultra-supercritical power plants, Ni-base alloys are prime candidate materials for long-term, high temperature applications, operating at temperatures and pressures as high as 750°C and 35 MPa. Alloy IN740 and its modification, alloy IN740H, are materials considered for such applications. Their microstructural evolution, at 750°C for times ranging between 3000 and 5000 h, has been investigated by means of scanning electron microscopy (FEGSEM), electron back-scattered diffraction (EBSD), energy dispersive X-ray (EDX) analysis and phase quantification. All the phases present in the two alloys were identified and quantified allowing comparison between the two microstructures, their evolution and stability. Particular attention is paid to gamma prime, η and G phase. The results obtained are used within a broader investigation whose aim is the improvement and further development of a predictive creep model based on continuous damage mechanics (CDM) which can forecast the alloy creep life.

Keywords: IN740, IN740H, Ni-base alloys, ultra-supercritical power plant, high-temperature, microstructural evolution, creep

1. INTRODUCTION

In the field of coal power generation, the drive for environmental protection has led to the engineering of more efficient power stations in conjunction with carbon capture technology. New advanced ultra-supercritical (USC) power plants are, therefore, being developed with the aim of operating with a steam temperature as high as 750°C and pressures of 35 MPa [1,2]. Ni-base alloys are amongst the candidate materials for applications such as boilers, able to withstand such service conditions. Such high temperature applications led the research focus on high creep resistance. Forecasted requirements in the power

generation sector have set the targets to minimum creep strength of 100 MPa at 100000 h of service [1-7]. Two possible candidate materials for USC boiler applications are the high chromium Ni-base precipitation-hardenable superalloy IN740 and its modification, IN740H, both developed by Special Metals [5, 7, 8-15]. The alloy IN740H has been produced with the desire of improving the IN740 high temperature properties (e.g. creep resistance). Compared with IN740, the Ti/Al ratio in IN740H is lowered in order to stabilise the microstructure at long ageing times. In addition, the Nb content is lowered to improve the weldability. The present investigation concentrates on characterising and comparing the high temperature microstructural evolution of the two alloys. Alloy IN740 has been aged at 750^{o}C for 3000h. Alloy IN740H has been aged at 750^{o}C for 5000h. Although the annealing conditions and ageing time for the aged IN740H specimens are different than that of its parent alloy, in view of the unchanged precipitation sequence within the annealing and ageing conditions [16], the comparison of the two microstructures does nonetheless provide a clear microstructural indication of several improvements. The analysis provides characterisation of the microstructural constituents and the quantification of phase fractions, mean particle size and inter-particle spacing (IPS). The quantitative data obtained through the microstructural analyses also serve as input and validation for modelling predictions. Although the ageing times are shorter than the aimed service life, in the absence of experimental data for such times, the data gathered are nonetheless very useful as they represent a way to assess the key parameters needed to develop the predictive model. The model uses a continuum damage mechanics (CDM) approach which has been successfully used for the prediction of creep rupture properties of 9 wt.%-Cr ferritic steel [17, 18] and which is now being adapted to the case of Ni-base superalloys systems. The modelling results are presented conjunctively in another publication [16]

2. EXPERIMENTAL PROCEDURE

The measured chemical composition of the alloys studied in this investigation is listed in Table 1. Notably, the contents of Al and B in IN740H have been increased, whilst the content of Nb has been decreased.

The IN740 samples were investigated in the as-received (AR) solubilised state (1170°C for 20 min - this specimen will be referred to as sample ref-AR) and in the aged condition. The ageing treatment was: isothermal holding at 750°C for 3000 h (this specimen will be referred to as ref-aged). The IN740H samples were

investigated in the AR state (1150°C for 1 hour - this sample will be referred to as sample H-AR) and in the aged condition. The ageing treatment was: isothermal holding at 750°C for 5000 h (this specimen will be referred to as sample H-aged). Alloy IN740H also underwent a pre-service ageing conditions of 4 hours at 750^{o}C allowing γ' precipitation.
Cutting of the samples was carried out using a Struers Accutom-5 cutting machine. Bakelite mounting for all samples was carried out in a Struers ProntoPress-10 machine. A Struers TegraPol-25 automatic polishing machine was used for both grinding and polishing. The latter was carried out with a 6μm and finally 1μm particle size diamond solution. Colloidal silica polishing was carried out for electron back-scatter diffraction (EBSD) analysis. Glyceregia (a mixture of glycerine, HCl and HNO_3) was used as etching reagent for preparing the samples to reveal the microstructural features. A LEO 1530VP field emission gun scanning electron microscope (FEG-SEM) was used to image the sample surfaces. The most useful detection mode for this analysis was high resolution secondary electron referred to as In-lens. Energy dispersive X-ray analysis (EDX) was performed in the FEG-SEM system using an Oxford Instruments X-Max 80mm^2 detector. Elemental mapping and point spectra were obtained for all the samples. EBSD analysis provided grain size and morphology. The system uses HKLNordlys F high speed Camera and Oxford Instrument Aztec EDX/EBSD microanalysis software for data collection. The grain size was also confirmed by using the mean linear intercept method. The Σ3 twin boundaries were not considered when determining the grain size.
Phase quantification, particle size and IPS analyses were carried out on all the samples investigated according to the method described elsewhere [19].

3. RESULTS AND DISCUSSION

3.1 Microstructural analysis of alloy IN740 specimens

The average grain size of the IN740 specimens is listed in Table 2. The grain structure of the ref-AR specimen can be observed in Figure 1: this appears uniform and it remained stable throughout the ageing treatment.

An example of elemental mapping of the ref-AR sample is shown in Figure 2.

It shows the presence of Nb- and Ti-rich MX precipitates which are expected to eventually transform to $M_{23}C_6$, η (Ni_3Ti), and G phase (a complex $Ni_{16}Nb_6Si_7$ silicide) upon ageing (Figure 3a). The limited presence of Si-enriched regions

has also been revealed and it has been linked to possible early onset of G phase nucleation and growth. High-magnification SEM imaging reveals the presence of very fine $M_{23}C_6$ particles (10-20 nm) nucleating at the grain boundaries, and the presence of very fine γ' (< 10nm) particles nucleating in the matrix (Figure 3b).

The predicted precipitation sequence performed for ref-aged is the following and it has been confirmed by the microstructural analysis[16]:

$$MX, \gamma' - G \text{ phase} - M_{23}C_6 - \eta$$

Both G phase and $M_{23}C_6$ volume fractions increase with ageing time, whilst MX volume fraction decreases with increasing η volume fraction.

The EDX analysis performed on ref-aged shows representatively all the phases encountered in the aged sample. In Figure 4 it can be observed that with ageing, the fine Cr-rich $M_{23}C_6$ decorating the GBs in the REF-AR material grow towards the formation of a semi-continuous film in both twin and grain boundaries. The large transitional MX particles evolve towards the formation of η, $M_{23}C_6$ and G phase. The fraction of the latter appears to be comparable to that of $M_{23}C_6$ particles. It is usually found in regions where the Cr rich $M_{23}C_6$ also develop. The benefit of such phase at low volume fractions is still controversial although it is generally accepted that its absence is preferable [10-12]. At 750°C the presence of η phase becomes a factor to strongly take into account. In fact, the Widmanstätten platelet morphology is observed after 3000 h and although the η volume fraction is still relatively low, significant increase of the phase volume fraction and dimensions is expected after longer ageing times at the expense of γ', reducing the beneficial effects of γ' on the alloy's mechanical properties [8,10-12].
The phases identified were therefore: a matrix of γ grains; a uniform dispersion of γ' particles; large globular primary MX formed in the microstructure prior to ageing and presenting the typical alignment caused by thermo-mechanical processing; a population of $M_{23}C_6$ nucleated at GBs, twin boundaries, on MX particles and intra-granularly; a relatively small fraction of η precipitates, whose morphology becomes also acicular at 750°C, mainly nucleated on GBs and on MX particles; Si-rich G phase, partially mixed with $M_{23}C_6$ precipitates, nucleating on MX, GBs and, to a lesser extent, intragranularly. Figure 5 shows selected examples of the microstructural constituents' morphology in the aged IN740 samples.

3.2 Microstructural analysis of alloy IN740H specimens

The average grain size of the IN740H specimens is listed in Table 3. The grain structure of the H-AR specimen can be observed in Figure 6: this appears uniform and it remained stable throughout the ageing treatment.

The chemical analysis of the H-AR sample, an example of which is shown in Figure 7, shows Ti- and Nb-rich MX located at grain boundaries. At high magnification the Cr-rich grain boundary precipitates can be detected and therefore identified as $M_{23}C_6$. The large MX shows the presence of Si enrichment only in the portion which is also rich in Nb. The portion of MX providing darker contrast (indicating Ti enrichment) is not enriched with Si. The formation of G phase necessitates the interaction of both Si and Nb. The finding suggests that the formation of G phase will be promoted at this transitional MX site.

The low magnification FEGSEM examination of the H-AR material shows an equiaxed grain structure with twins clearly visible throughout the whole microstructure. The following images in Figure 8 show the main microstructural features present in the sample H-AR.

Large precipitates are visible, whose morphology and contrast are consistent with MX particles present in the alloy prior to the pre-service heat treatment. They are mainly located at GBs. The matrix is uniformly dispersed with fine γ' particles, precipitated during the pre-service ageing treatment. The grain boundaries are decorated with precipitates for almost their full length. They form a semi-continuous film which is mostly made of Cr-rich $M_{23}C_6$ carbides (bright contrast), as discussed in the chemical analysis section. Twin boundaries also are almost completely decorated by fine $M_{23}C_6$ particles. At higher magnification the dispersion of intra-granularly precipitated γ' particles becomes clearly discernible.

The predicted precipitation sequence performed for sample aged-H is the following and it has been confirmed by the microstructural analysis [16]:

$$MX, \gamma' - G \text{ phase} - M_{23}C_6$$

G phase and $M_{23}C_6$ volume fractions increase with ageing time although the predictions appear to overestimate the G phase volume fraction. The η precipitation has been suppressed.

The chemical analysis of the aged sample aged-H (Figure 9) shows Ti-rich MX both intra- and inter-granularly. The grain boundaries are enriched with Cr, indicating the precipitation of $M_{23}C_6$. It also appears that the large MX located at GBs act as nucleation sites for the Cr-rich $M_{23}C_6$ precipitates. The presence of η phase, either in the acicular morphology or in the blocky morphology, which usually develops as transformation products of MX transition at high temperature, has not been encountered.
Figure 10 shows the high magnification EDX mapping performed on a large MX precipitate and the adjacent GB. It is clear that at this temperature, the development of G phase (enriched in Si and Nb) is favoured at MX site.

The phases identified were therefore: a matrix of γ grains; a uniform dispersion of γ' particles; large globular primary Ti- and Nb-rich MX formed in the microstructure prior to ageing; a population of $M_{23}C_6$ nucleated at GBs, twin boundaries, on MX particles and intra-granularly; initiation of Si-rich G phase, suggested by Si- and Nb-rich regions of MX particles. Figure 11 shows selected examples of the microstructural constituents' morphology in the H-aged samples.

These microstructural findings for both aged samples are summarised in Table 4.

3.3 Phase quantification and IPS analysis

The microstructure of the aged specimens has been quantified. The phase quantification results as well as the inter-particle spacing and the average particle size, obtained for both aged specimens, are shown in Table 5. This activity provides several advantages: it helps quantifying the effects of thermal treatments on the alloy (e.g. γ' precipitation and coarsening), and it provides data which can be used as input and validation for predictive models. The inter-particle spacing for the GB particles is also calculated taking into account the elliptical approximation utilised in the case of a semi-continuous film [19].

3.4 Conclusions from the comparison between IN740H and IN740H microstructures

The extent of the G phase encountered in specimen aged-H appears to be lower than that of specimen ref-aged. The compositional change of specimen aged-H also causes the fraction of γ' to decrease. The dimensions of γ' are coarser than those found in specimen ref-aged but this is mostly caused by the difference in ageing time.

It is important to highlight the suppression of any visible η formation and the lower G phase fraction observed in specimen aged-H, in comparison to its parent IN740 alloy. Beside the lower γ' content, this appears to be one of the best improvements in alloy IN740H. It is also very possible that the fraction of G phase will undesirably increase with increasing ageing time. Longer ageing times should be investigated in order to assess the effects on the microstructure of alloy IN740H.

IN740H has been successfully developed to achieve better high temperature performance by decreasing the fraction of phases which are detrimental to the creep properties of the alloy. In particular, acicular η phase (growing at the expenses of γ') is connected to higher creep susceptibility by making crack initiation and propagation more favourable.

REFERENCES

[1] R. Viswanathan, W. Bakker: "Materials for Ultrasupercritical Coal Power Plants-Boiler Materials", Part 1. *Journal of Materials Engineering and Performance,* Vol. 10 (2001), pp. 81–95

[2] T. B. Gibbons: "Superalloys in modern power generation applications", *Materials Science and Technology,* Vol. 25 (2009), pp. 129–135

[3] A. Sharma, B.J J. P. Buhre, S. Richardson, C. Spero, T. Wall: "Fired Supercritical Boilers Operational Issues and Coal Quality Impacts", Technical Note 20. *CCSD(Cooperative Research Centre for Coal in Sustainable Development) Report*, 2002.

[4] R. Viswanathan, J. F. Henry, J. Tanzos, G. Stanko, J. Shingledecker, B. Vitalis, R. Purgert*:* "U.S. Program on Materials Technology for Ultra-Supercritical Coal Power Plants", *Journal of Materials Engineering and Performance* Vol. 14 (2005), pp. 281–292

[5] R. C. Reed: "*The Superalloy Fundamentals and Applications*" (Cambridge University Press, 2006)

[6] J. P. Shingledecker, R. W. Swindeman, Q. Wu, V.K. Vasudevan: "Creep Strength of High Temperature Alloys For Ultra-supercritical Steam Boilers", *4th EPRI Conference on Advances in Materials Technology for Fossil Power Plants,* 2007

[7] M. J. Donachie, S. J. Donachie: *SUPERALLOYS A Technical Guide*. (ASM International: 2002)

[8] N. D. Evans, P. J. Maziasz, R. W. Swindeman, G. D. Smith: "Microstructure and phase stability in INCONEL alloy 740 during creep", *Scripta Materalia,* Vol. 51 (2004), pp. 503-507

[9] J. P. Shingledecker, N. D. Evans, G. M. Pharr: "Influences of composition and grain size on creep-rupture behaviour of Inconel alloy 740", *Materials Science and Engineering A,* Vol. 578 (2013), pp. 277-286

[10] S. Zhao, X. Xie, D. G. Smith, S. J. Patel: "Research and improvement on structure stability and corrosion resistance of nickel-base superalloy INCONEL alloy 740", *Materials and Design,* Vol. 27 (2006), pp. 1120-1127

[11] C. J. Cowen, P. E. Danielson, P. D. Jablonski: "The microstructural evolution of Inconel alloy 740 during solution treatment, aging, and Exposure at 760^0C", *Journal of Materials Engineering and Performance,* Vol. 20 (2011), pp. 1078-1083

[12] J.-H. Oh, I-.C. Choi, Y.-J. Kim, B.-G. Yoo, J.-I. Jang: "Variations in overall- and phase-hardness of a new Ni-based superalloy during isothermal ageing", *Materials Science and Engineering A,* Vol. 528 (2011), pp. 6121-6127

[13] S.J. Patel, J.J. deBarbadillo, B.A. Baker, R.D. Gollihue: "Nickel base superalloys for next generation coal fired AUSC power plants", *Procedia Engineering,* Vol. 55 (2013), pp. 246-252

[14] C. Yan, L Zhengdong, A. Godfrey, L. Wei, W. Yuqing: "Microstructure evolution and mechanical properties of Inconel 740H during aging at 750^oC", *Materials Science and Engineering A,* Vol. 589 (2014), pp. 153-164

[15] J. Wang, J. Donh, M. Zhang, X. Xie: "Hot working characteristics of nickel-base superalloy 740H during compression", *Materials Science and Engineering A,* Vol. 566 (2013), pp. 61-70

[16] R.G. Faulkner, S.Vujic, F. Di Martino, and S.C. Hogg, "Modelling of Creep and Fracture Properties of Nickel Based Alloys 740 and 740H", submitted for publication

[17] Y. F. Yin, R. G. Faulkner, "Continuum damage mechanics modelling based on simulation of microstructural evolution kinetics", *Materials Science and Technology,* Vol. 22, n. 8 (2006), pp.929-936

[18] B. Dyson: “Use of CDM in marerials modelling and component creep life prediction”, *Journal of Pressure Vessel Technology*, Vol. 122 (2000), pp. 281-296

[19] S. F. Di Martino, R. G. Faulkner and S. C. Hogg, “Characterisation of microstructure and creep predictions of alloy IN740 for ultrasupercritical power plants”, *Materials Science and Technology* 2014; 31(1), 48-58.

Acknowledgements

The investigation is part of the collaborative project ENER/FP7EN/249809/MACPLUS, funded by the EU within the FP7 framework. Special thanks to S. McCoy (Special Metals) for providing the samples

TABLES

Alloy	*Chemical composition weight %*												
	C	***Mn***	***Si***	***Al***	***Cr***	***Cu***	***Co***	***Mo***	***Fe***	***Ti***	***Nb***	***B***	***Ni***
IN740	0.034	0.3	0.58	1.04	24.5	--	19.8	0.6	0.45	1.64	2.4	--	*Bal*
IN740H	0.03	-	0.15	1.35	25	-	20	0.5	-	1.35	1.5	0.001	Bal.

Table 1: Compositions of IN740 amd IN740H alloy investigated

Average grain size (μm)	
ref-AR	ref-aged
69 ± 30	72 ± 34

Table 2: average grain size for the IN740 specimens

Average grain size (μm)	
sample H-AR	H-aged
83	90

Table 3: average grain size for the IN740H specimen

Precipitate	Location	Morphology	Remarks	Ref-aged	H-aged
γ’	Intragranular	Cuboidal	Clearly observed after etching. Uniformely distributed.	✓	✓
MX	Intragranular GBs; Randomly distributed	Cuboidal Globular Irregular	MX precipitates mainly formed during solidification. After long high temperature exposure, a large amount of MX were observed to have transformed into other phases	✓	✓
$M_{23}C_6$	GBs Intragranular (smaller fraction)	Globules Film Platelet Cellular Irregular	This carbide was usually found at grain and twin boundaries. It is common also to find them nucleating on the MX precipitates	✓	✓
G phase	GBs Intragranular (smaller fraction) Nucleating on MX Mixed with $M_{23}C_6$	Globules; Cellular; Irregular	Si-rich G phase was found precipitating near $M_{23}C_6$ carbides, or even mixed with $M_{23}C_6$. It is difficult to distinguish the two wihtout the aid of EDX analysis. G phase was also found	✓	✓

			nucleating on MX		
η	Intragranular (small fraction) GBs Nucleating on MX Nucleating on or nearby $M_{23}C_6$	Acicular platelet Cellular Globules Irregular	η phase was only found in alloy IN740. Its fraction was significant at 750ºC, displaying after 3000 h the typical acicular morphology developing towards the interior of the grains at the expenses of γ’	✓	X

Table 4: Summary of phases present in 1 and 1H aged samples

Specimen	**γ' Area Fraction (%)**	**Other Precipitates Area Fraction (%)**	**γ' Average Size (nm)**		**Other Precipitates Average Size (µm)**	**GB Precipitates Average Size (µm)**	**γ' IPS (nm)**		**GB Particles IPS (µm)**
			d	**s**			**d**	**s**	
Ref-aged	26 ± 1.4	2.6 ± 0.09	134 ± 9	118 ± 9	0.69 ± 0.04	0.91 ± 0.09	101 ± 8	90 ± 8	0.3 ± 0.02
H-aged	18 ± 1.5	2.4 ± 0.09	129 ± 9	114 ± 9	3 ± 0.09	2.1 ± 0.1	274 ± 14	272 ± 14	0.17 ± 0.01

Table 5: Phase quantification results as well as inter-particle spacing and average particle size, obtained for both aged specimens

FIGURES

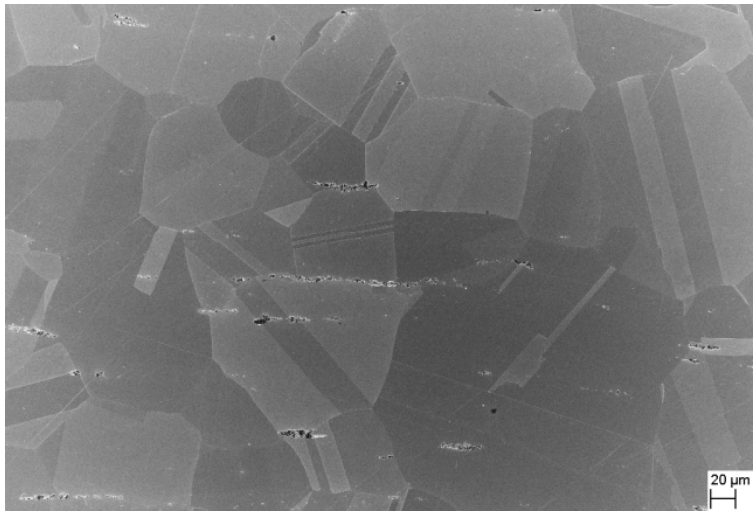

Figure 1: Low magnification image of ref-AR sample

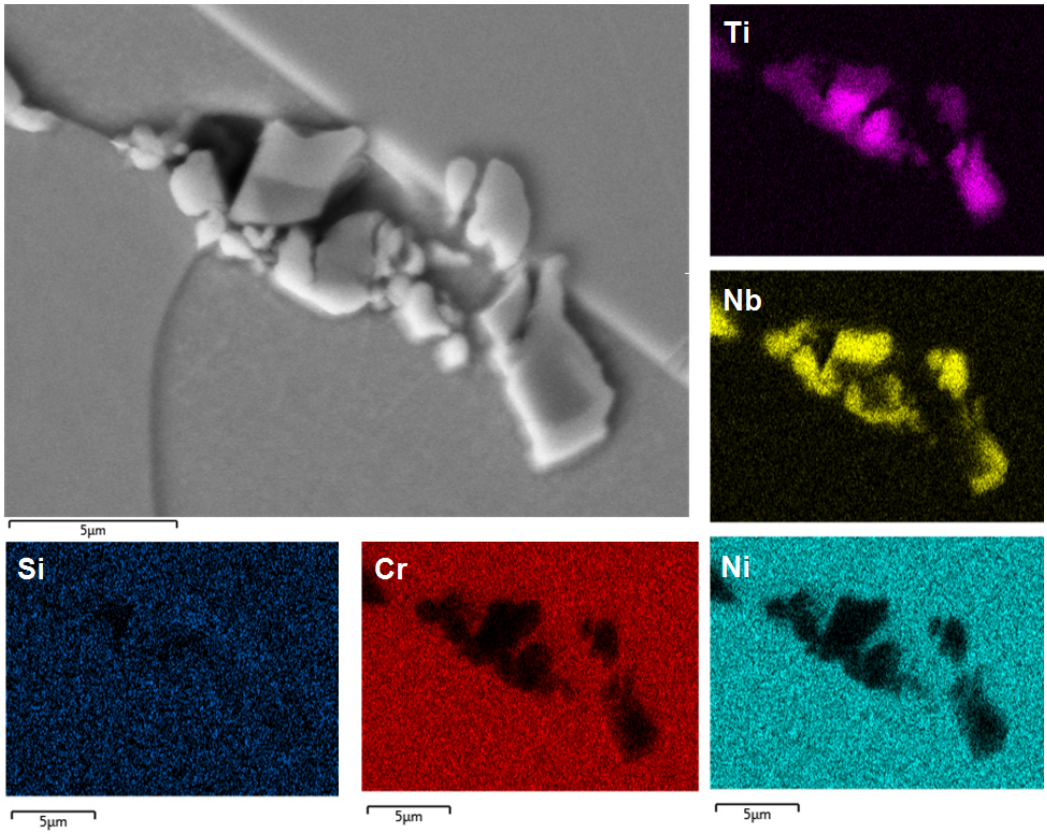

Figure 2: EDX map of IN740 as-received specimen showing Ti- and Nb-rich MX precipitate

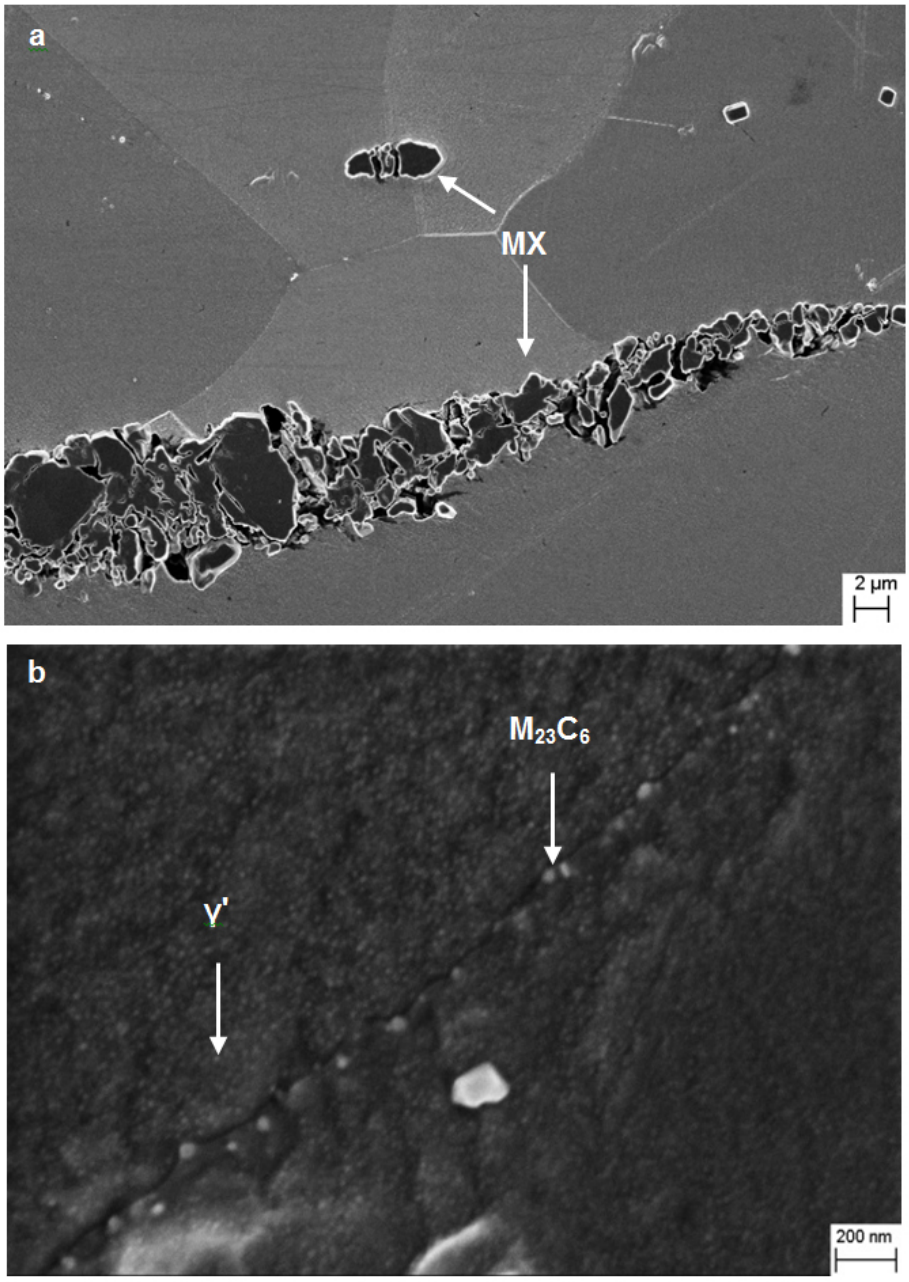

Figure 3: (a) Large and small primary MX (Ti- and Nb-rich) precipitates; (b) High magnification image of the $M_{23}C_6$ particles nucleating at the GB and the extremely fine γ' particles nucleating and beginning to coarsen in the matrix

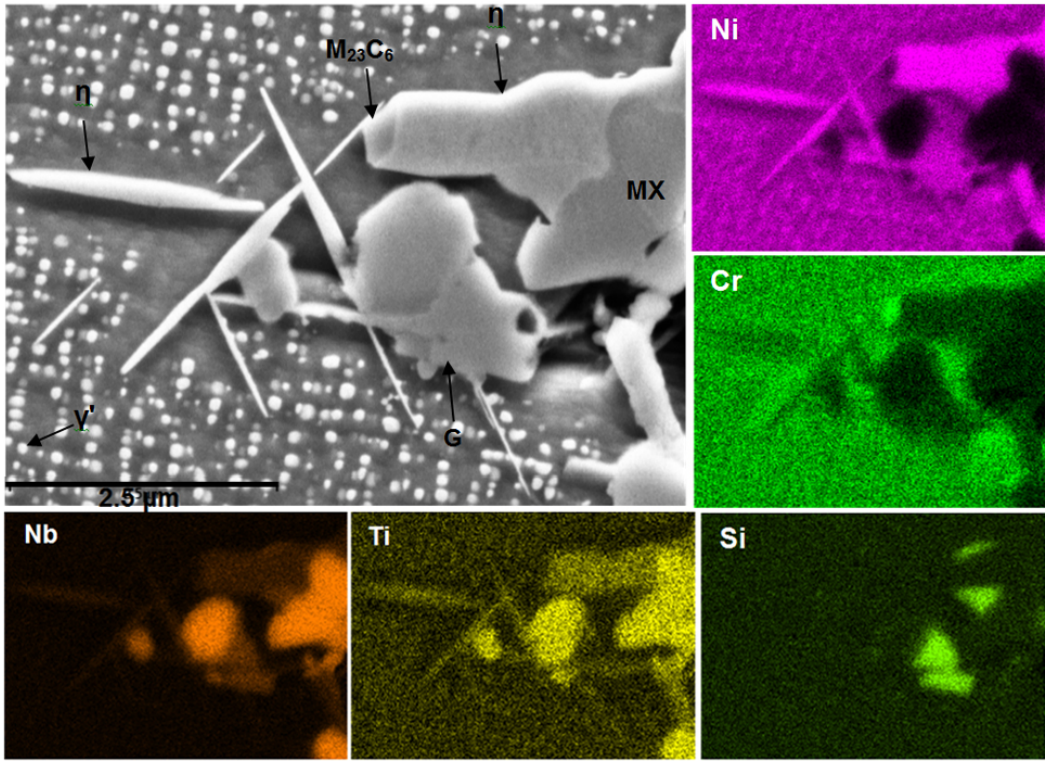

Figure 4: SE2 image and EDX mapping analysis carried out on ref-aged showing MX (Ti- and Nb-rich) precipitate evolving into η, G and $M_{23}C_6$, blocky and acicular η (Ni-rich), γ' (Ni-rich), G phase (Si- and Nb-rich), $M_{23}C_6$ (Cr-rich)

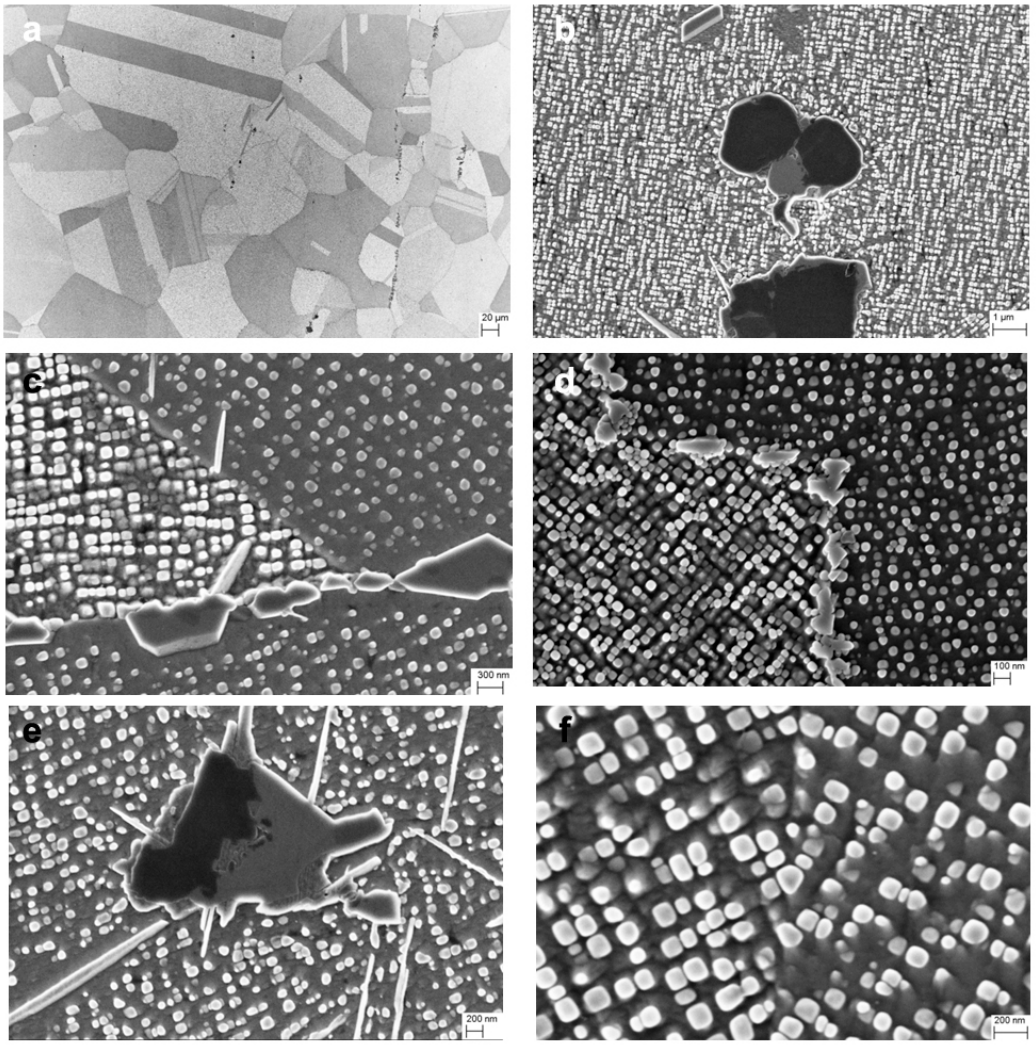

Figure 5a-f: *(a,b) low magnification in-lens SEM image of the aged ref-aged showing the general grain structure, twins and large MX particles and η phase; (c) $M_{23}C_6$ and η particles at grain boundaries and different γ' orientation ; (d) $M_{23}C_6$ particles decorating twin boundary; (e) transition MX particle decorated by acicular η phase; (f) different γ' orientation at twin boundary*

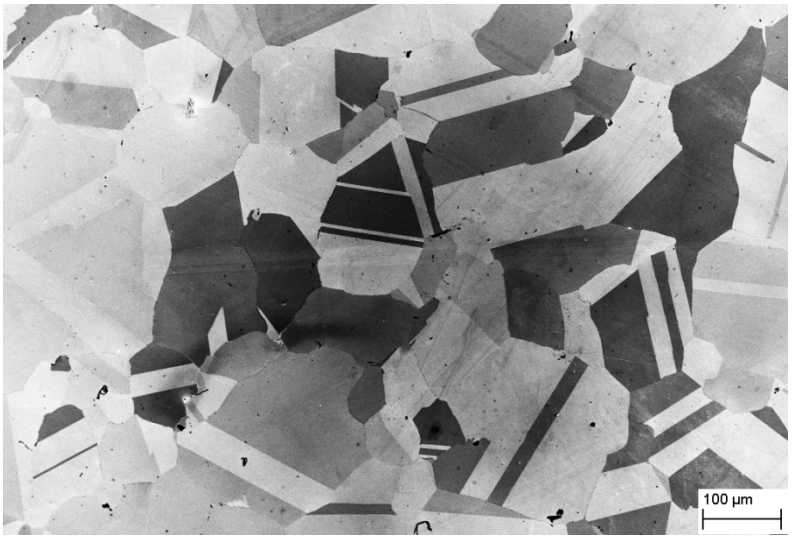

Figure 6: Low magnification image of sample H-AR

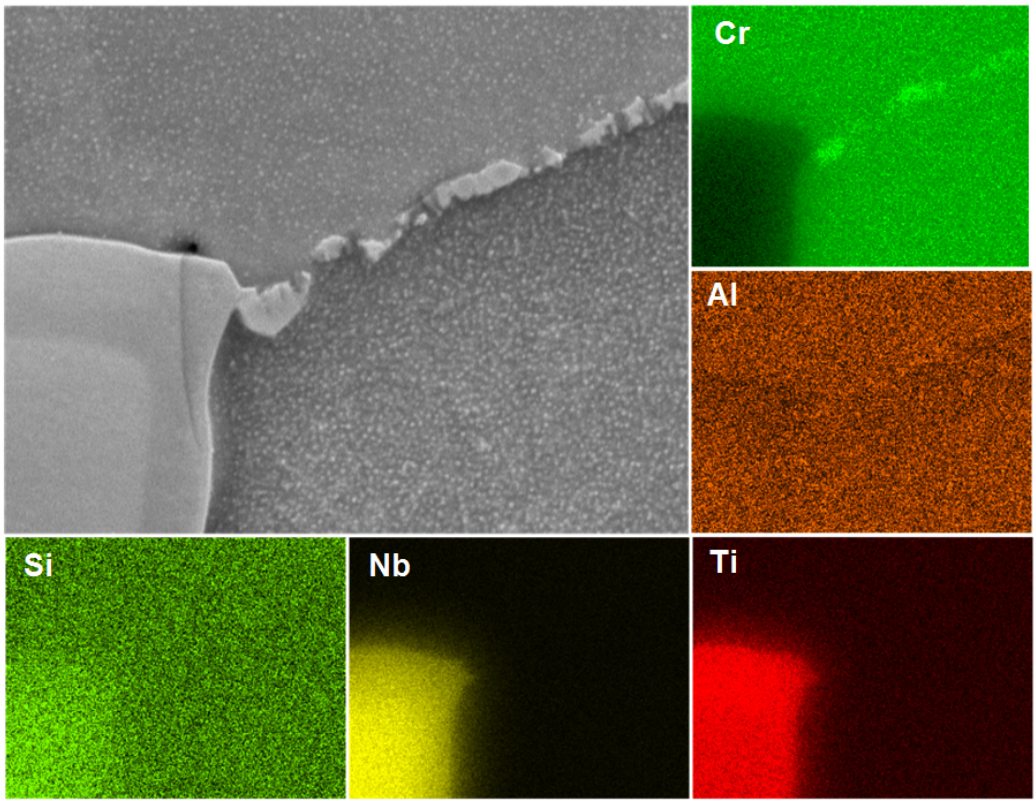

Figure 7: *SEM image and elemental maps for H-AR sample showing a Ti- and NB-rich MX precipitate and Cr-rich $M_{23}C_6$ precipitates located at GBs*

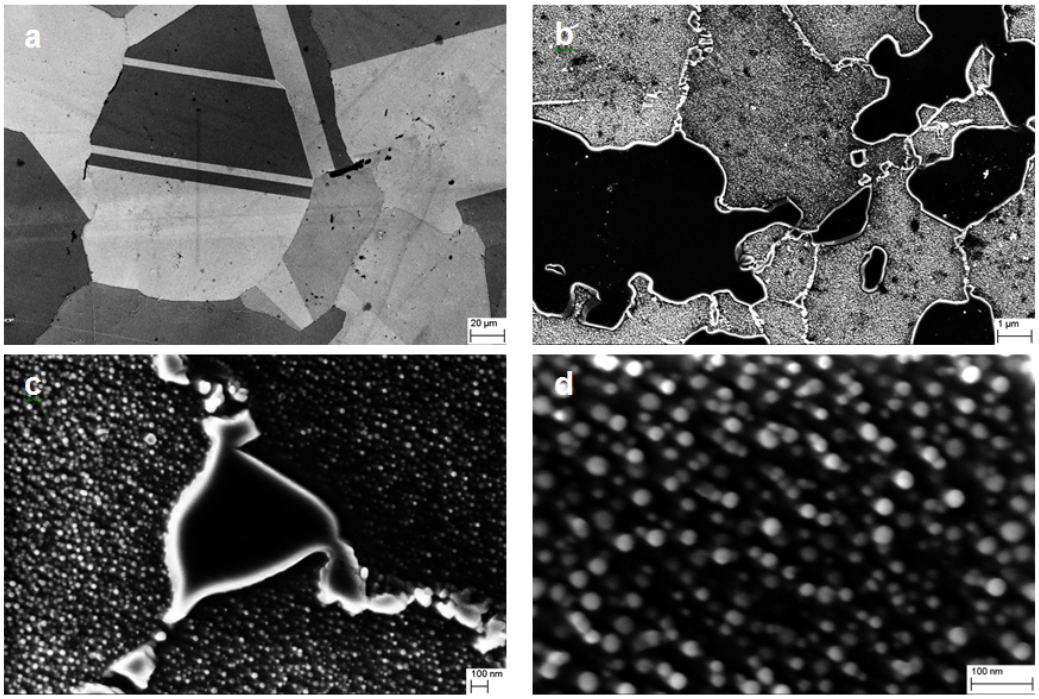

Figure 8a-d: *(a,b) low magnification in-lens SEM image of the H-AR specimen showing the general grain structure, twins and large MX particles (dark contrast);(c) $M_{23}C_6$ particles at grain boundaries; (d) fine γ' particles*

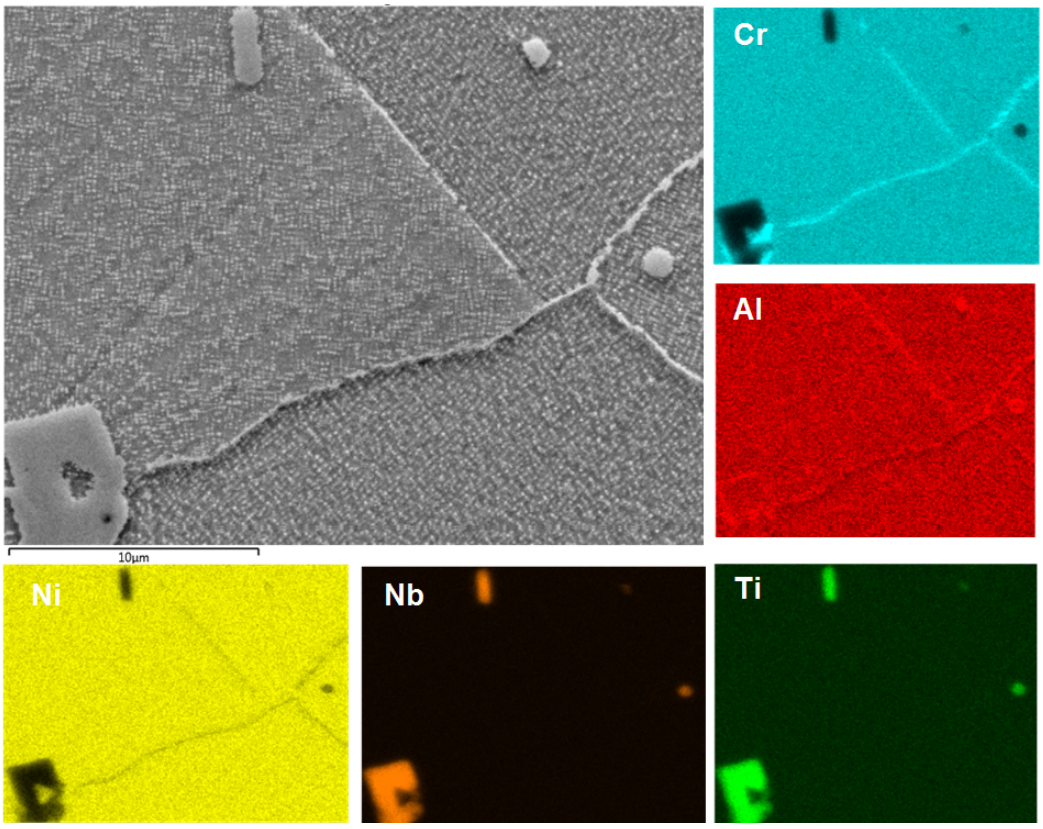

Figure 9: *SEM image and elemental maps for the 1H specimen showing a Ti-rich MX precipitates, Cr-rich $M_{23}C_6$ precipitates located mainly at GBs*

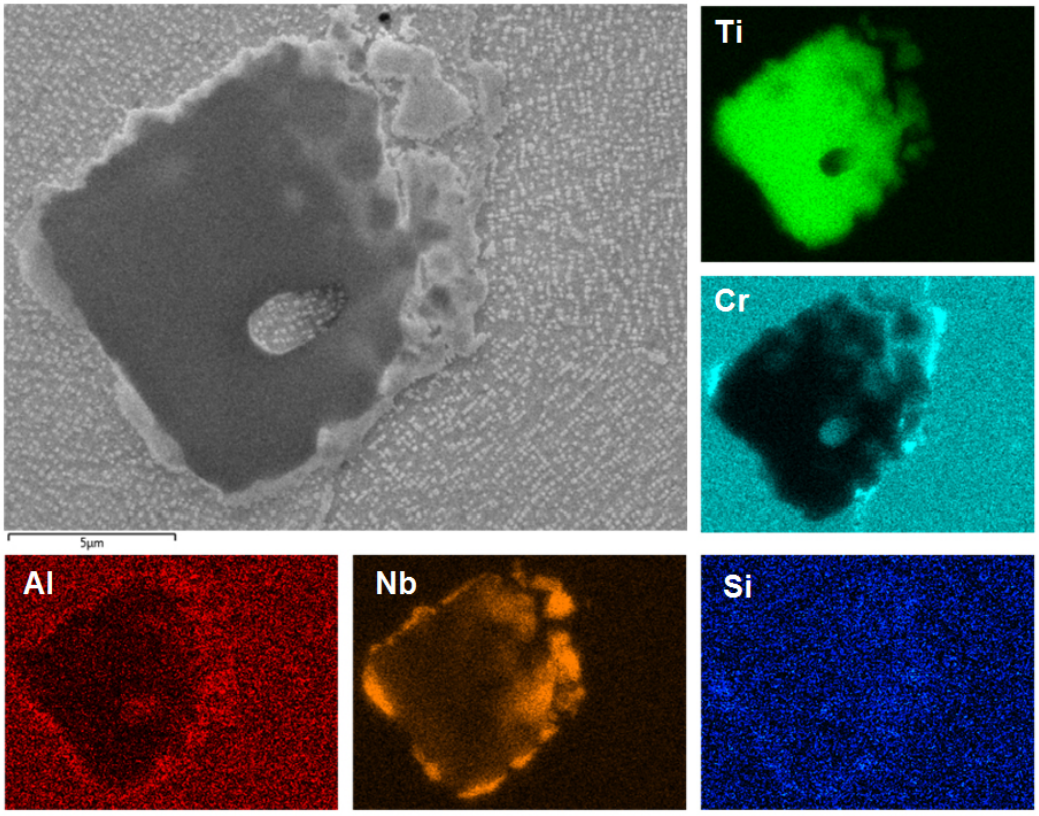

Figure 10: *SEM image and elemental maps for the 1H specimen showing a Ti-rich MX precipitate, Cr-rich $M_{23}C_6$ precipitate developing at the MX site, and Nb-rich G phase developing at the MX site*

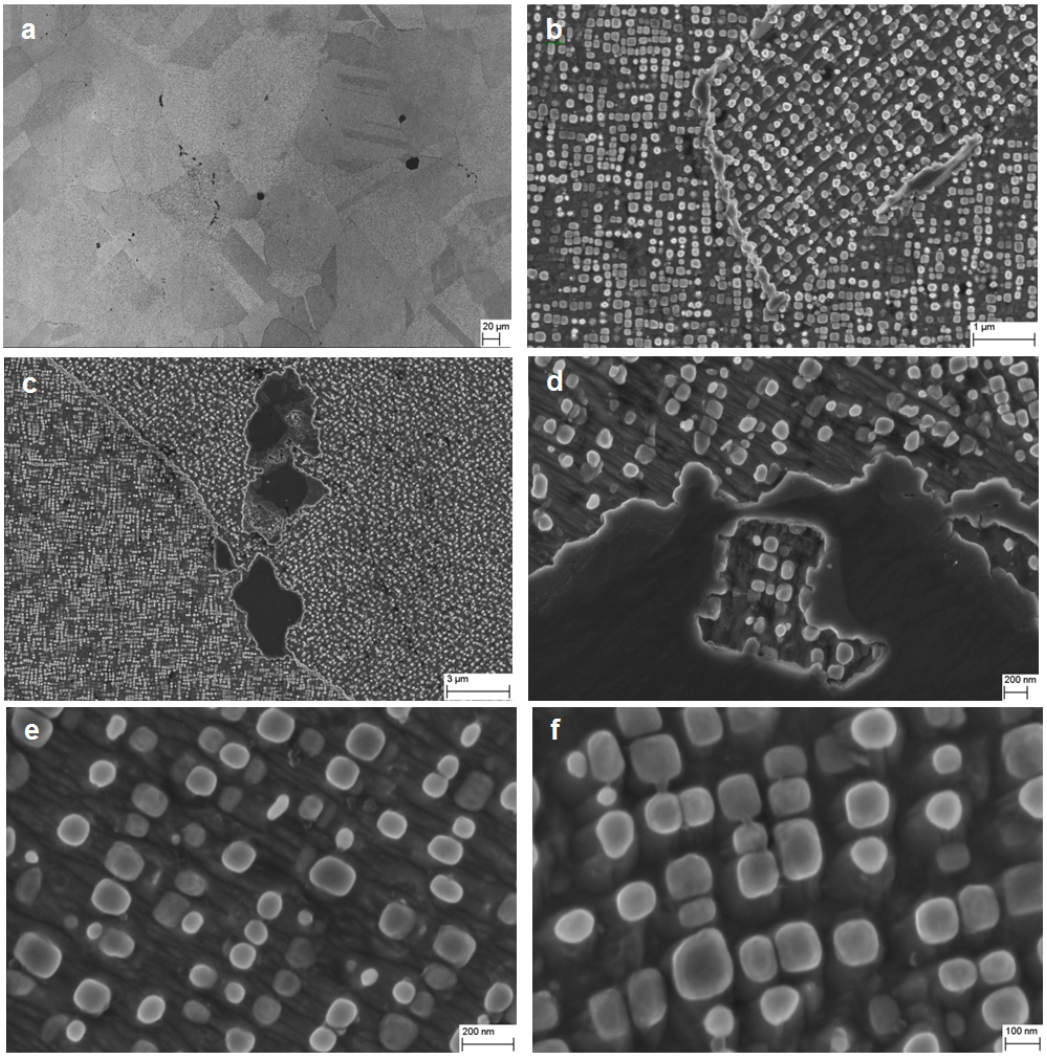

Figure 11a-: *(a) low magnification SEM image showing the grain structure of H-aged; (b) Grain boundary containing $M_{23}C_6$ and possibly G phase;(c) Large Ti-rich MX (dark contrast) transforming into G phase and $M_{23}C_6$; (d) High magnification of Ti-rich MX transforming into G phase and $M_{23}C_6$, surrounded by γ' particles (e,f) γ' particles*